JPE

Performance Analysis of a Stand-alone Brushless Doubly-fed Induction Generator Using a New T-type Steady-state Model

Yi Liu*, Wei Xu†, Gang Zhi**, and Junlin Zhang*

*School of Mechanical and Electrical Engineering, Huanggang Normal University, Huanggang, China
†State Key Laboratory of Advanced Electromagnetic Engineering and Technology, School of Electrical and Electronic Engineering, Huazhong University of Science and Technology, Wuhan, China
**China Changjiang National Shipping Group Motor Factory, Wuhan, China

Abstract

The brushless doubly-fed induction generator (BDFIG) is a new type of dual stator winding induction generator. In such a generator, both the power winding (PW) and the control winding (CW) are housed in the stator. This paper presents the performance characteristics of a stand-alone BDFIG operation system. A new T-type steady-state model of a BDFIG is proposed. This model is more suitable for the performance analysis of stand-alone BDFIGs than the conventional Π-type steady-state model and the simplified inner core steady-state model. The characteristics of the power flow and CW current are analyzed by detailed mathematical derivations on the basis of the proposed T-type steady-state model. The analysis results are verified by experiments, which are carried out on a prototype BDFIG. The results of the performance analysis contribute to simplifying the control circuit, improving the control performance, and selecting an appropriate BDFIG for actual industrial applications.

Key words: brushless doubly-fed induction generator (BDFIG), performance analysis, stand-alone generation system, T-type steady-state model

I. INTRODUCTION

A BDFIG can output voltage with a constant frequency while the rotor speed and load are changing, which makes the BDFIG suitable for variable speed power generation in both grid-connected and stand-alone applications, such as wind power generation and ship shaft power generation.

Generally, a grid-connected generation system controls the generator's active and reactive power. Nevertheless, in a stand-alone generation system, the amplitude and frequency of the output voltage of the generator should be stabilized when the rotor speed or load changes. Therefore, the operation characteristics of a grid-connected BDFIG are different from those of a stand-alone BDFIG. The control design and performance analysis for BDFIGs used in grid-connected wind generators were developed in [1-4]. For stand-alone power generation applications, some control strategies and analysis have been developed [5-8], which are suitable for DFIGs but not for BDFIGs. No other reports on BDFIG applications in the stand-alone power generation have been found in the literature expect for [22] and [23].

Many control strategies have been proposed for BDFIGs, such as open-loop scalar voltage control [9], closed-loop scalar current control [10], phase-angle control [11], closed-loop scalar frequency control [12], indirect stator-quantities control [13], and direct torque control [14].

Design theories and mathematical models of BDFIGs have been studied in [15]-[21]. The most well-known steady-state models of BDFIGs are the Π-type model and the simplified inner core model. However, the Π-type steady-state model is too complex for BDFIG performance analysis, and the inner core steady-state model is not suitable for the analysis of stand-alone BDFIG operation systems since it omits too many parameters.

In this paper, a new T-type steady-state model for BDFIGs is presented. The power flow and CW current in stand-alone BDFIG operation systems are analyzed by using the T-type steady-state model. Experimental investigations are implemented on a prototype BDFIG, which is specially designed for the application of stand-alone shaft generation in cargo ships driven by a fixed pitch propeller. The experimental results confirm the validity of the analysis. The performance analysis results are helpful for simplifying the control circuit, improving the control performance, and selecting an appropriate BDFIG for actual industrial applications.

II. Basic Operation Principle of the BDFIG

A BDFIG can be operated in several modes, including synchronous mode, cascade mode, and induction mode [18]. The synchronous mode, also called the doubly-fed mode, is the optimal mode among three operation modes. Under this mode, the rotor speed can be expressed as follows:

$$\omega_r = \frac{\omega_1 + \omega_2}{p_1 + p_2} \tag{1}$$

where p is the pole pairs, and ω the angular frequency. The subscripts 1, 2, and r indicate the PW, CW, and rotor, respectively.

When ω_2 is zero, the rotor is rotating at the so-called natural synchronous speed ω_N. The rotor of the BDFIG is driven by a prime mover, such as a diesel engine or a wind turbine. To keep ω_1 constant, ω_2 should be changed with variations of the rotor speed ω_r, and the expression of ω_2 can be deduced from Equ. (1):

$$\omega_2 = \omega_r(p_1 + p_2) - \omega_1 \tag{2}$$

It is noted that when the the BDFIG is operating below ω_N, the value of ω_2 is negative. On the other hand, when it is operating above ω_N, the value of ω_2 is positive. The phase sequence of the negative frequency voltage and the positive frequency voltage are opposite.

The slips for the PW and CW can be defined as [18]:

$$s_1 = \frac{\omega_1 - p_1\omega_r}{\omega_1} \tag{3}$$

$$s_2 = \frac{\omega_2 - p_2\omega_r}{\omega_2} \tag{4}$$

From Eqns. (1), (3), and (4), the relation between s_1 and s_2 can be derived as:

$$\frac{s_1}{s_2} = -\frac{\omega_2}{\omega_1} \tag{5}$$

III. Steady-state Models of the BDFIG

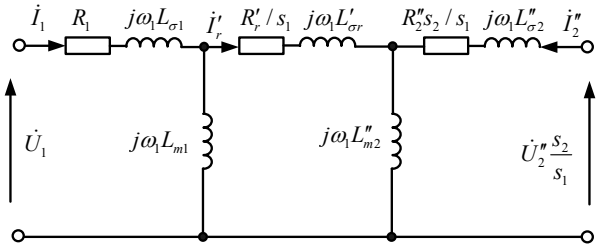

Fig. 1. Π-type steady-state model of a BDFIG.

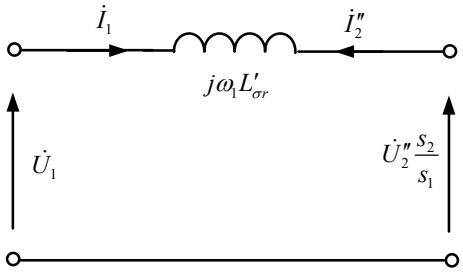

Fig. 2. Simplified inner core steady-state model of a BDFIG.

A. Conventional Π-Type Steady-state Model

Generally, the conventional Π-type steady-state model [18], [20], [21] in Fig. 1 can be used to express the steady-state operation of a BDFIG. In this model, all of the parameters are referred to the PW side, ignoring the BDFIG's iron loss. In Fig. 1, R_1, R_2'' and R_r' are the PW, CW and rotor resistances; L_{m1} and L_{m2}'' the PW and CW magnetizing inductances, $L_{\sigma 1}$, $L_{\sigma 2}''$ and $L_{\sigma r}'$ are the PW, CW and rotor leakage inductances; $\dot{U}_1$ and $\dot{U}_2''$ are the PW and CW phase voltage vectors; and $\dot{I}_1$, $\dot{I}_2''$ and $\dot{I}_r'$ are the PW, CW and rotor phase current vectors, respectively.

B. Simplified Inner Core Steady-state Model and its Defect

The inner core steady-state model for a BDFIG is proposed by McMahon *et al.* [18], as shown in Fig. 2. In this model the magnetizing inductances, the stator leakage inductances, and the stator and rotor resistances are neglected. The inner core model simplifies the steady-state analysis of the BDFIG to some extent.

From Fig. 2, it is can be seen that $\dot{I}_1 = -\dot{I}_2''$. In addition, it is known that $\dot{I}_1 = 0$ when the BDFIG is operating in the unloaded condition. Hence, it can be obtained that $\dot{I}_2'' = 0$ in the unloaded condition. However, an excitation current must be supplied to the CW to generate the PW voltage in practical applications. This means that the CW current $\dot{I}_2''$ cannot be zero when the stand-alone BDFIG is running. Therefore, the simplified inner core steady-state model does not fit the performance analysis of stand-alone BDFIGs.

C. Proposed T-type Steady-state Model

Actually, the Π-type steady-state model shown in Fig. 1 is

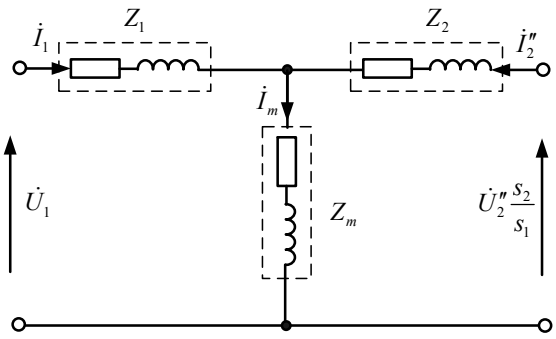

Fig. 3. T-type steady-state model of a BDFIG.

a passive linear two-port network, which can be equivalently transformed into a T-type steady-state model consisting of three impedances, as shown in Fig. 3 [24].

The parameters Z_1, Z_2, and Z_m in Fig. 3 are derived in the Appendix. The T-type steady-state model is also a two-port network and it is similar to the steady-state model of the regular asynchronous machine. It is noted that the T-type and Π-type steady-state models are almost equivalent since they both employ equivalent circuit transformations in the derivation process as described in the Appendix. According to the Appendix, the parameters Z_1, Z_2, and Z_m can be expressed as:

$$Z_1 = \frac{j\omega_1 L_{m1}((R_r'/s_1)+j\omega_1 L_{\sigma r}')}{j\omega_1 L_{m1}+(R_r'/s_1)+j\omega_1 L_{\sigma r}'+j\omega_1 L_{m2}''} + R_1 + j\omega_1 L_{\sigma 1} \quad (6)$$

$$Z_2 = \frac{j\omega_1 L_{m2}''((R_r'/s_1)+j\omega_1 L_{\sigma r}')}{j\omega_1 L_{m1}+(R_r'/s_1)+j\omega_1 L_{\sigma r}'+j\omega_1 L_{m2}''} + R_2''\frac{s_2}{s_1} + j\omega_1 L_{\sigma 2}'' \quad (7)$$

$$Z_m = \frac{j\omega_1 L_{m1} j\omega_1 L_{m2}''}{j\omega_1 L_{m1}+(R_r'/s_1)+j\omega_1 L_{\sigma r}'+j\omega_1 L_{m2}''} \quad (8)$$

To stabilize the operation of the BDFIG, the slip s_1 should be far away from zero [18]. Therefore, if the rotor resistance R_r' is ignored, the term R_r'/s_1 in Z_1, Z_2, and Z_m can also be ignored. Then the expressions of Z_1, Z_2, and Z_m can be simplified as:

$$Z_1 = j\omega_1(\alpha_1 + L_{\sigma 1}) + R_1 \quad (9)$$

$$Z_2 = j\omega_1(\alpha_2 + L_{\sigma 2}'') + R_2''\frac{s_2}{s_1} \quad (10)$$

$$Z_m = j\omega_1\alpha_3 \quad (11)$$

where $\alpha_1 = \frac{L_{m1}L_{\sigma r}'}{L_{m1}+L_{\sigma r}'+L_{m2}''}$,

$\alpha_2 = \frac{L_{m2}''L_{\sigma r}'}{L_{m1}+L_{\sigma r}'+L_{m2}''}$, $\alpha_3 = \frac{L_{m1}L_{m2}''}{L_{m1}+L_{\sigma r}'+L_{m2}''}$.

When the PW phase voltage and phase current used as input variables, and the referred CW phase voltage and phase current are used as output variables, the T-type steady-state model in Fig. 3 can be concisely expressed by a matrix equation as follows [24]:

$$\begin{bmatrix} \dot{U}_2''\frac{s_1}{s_2} \\ \dot{I}_2'' \end{bmatrix} = \begin{bmatrix} \frac{Z_2+Z_m}{Z_m} & -(Z_1+Z_2+\frac{Z_1Z_2}{Z_m}) \\ \frac{1}{Z_m} & -\frac{Z_1+Z_m}{Z_m} \end{bmatrix} \begin{bmatrix} \dot{U}_1 \\ \dot{I}_1 \end{bmatrix} \quad (12)$$

With its simple structure, the T-type steady-state model can be readily described by mathematical equations, which facilitates the subsequent derivation of the power and current of the BDFIG. It also provides a new approach to the performance analysis of stand-alone BDFIG systems.

IV. Performance Analysis of the Stand-alone BDFIG

A. Structure of the Stand-Alone BDFIG Operation System

The structure of a stand-alone BDFIG operation system is shown in Fig. 4. A prime mover is used to drive the rotor of the BDFIG. Two back-to-back PWM converters, a CW side converter (CSC) and a supply side converter (SSC), are connected between the PW and the CW with a LCL filter.

The CSC supplies the CW with a frequency-variable exciting current. The SSC with a LCL filter has two functions: (a) stabilizing the voltage of the DC bus at the setpoint, (b) achieving a bidirectional energy flow. The voltages and currents of the PW and CW, as well as the position of the rotor are all transmitted to the control system. They are measured by voltage sensors, current sensors, and an encoder, respectively. The PW voltage amplitude and frequency are kept constant under a variable rotor speed and load by appropriately adjusting the amplitude and frequency of the CW current.

B. Analysis of the Power Flow

From Fig. 3, it can be seen that:

$$\begin{cases} \dot{I}_1 Z_1 + \dot{I}_m Z_m + \dot{U}_1 = 0 \\ \dot{I}_2'' Z_2 + \dot{I}_m Z_m + \dot{U}_2'' s_2/s_1 = 0 \\ \dot{I}_m = \dot{I}_1 + \dot{I}_2'' \end{cases} \quad (13)$$

From Equ. (13), the PW phase current vector $\dot{I}_1$ and the CW phase current vector $\dot{I}_2''$ can be derived as:

$$\dot{I}_1 = \frac{-\dot{U}_1(Z_2+Z_m)+\dot{U}_2''s_2Z_m/s_1}{(Z_1+Z_2)Z_m+Z_1Z_2}$$

$$(14)\ \dot{I}_2'' = \frac{\dot{U}_1Z_m-\dot{U}_2''s_2(Z_1+Z_m)/s_1}{(Z_1+Z_2)Z_m+Z_1Z_2} \quad (15)$$

The PW active power P_1 and the CW active power P_2 are given by:

$$P_1 = 3\mathrm{Re}\{\dot{U}_1 I_1^*\} \quad (16)$$

$$P_2 = 3\mathrm{Re}\{\dot{U}_2''\dot{I}_2''^*\} \quad (17)$$

Substituting Eqns. (9)-(11) and (14) into Equ. (16), and

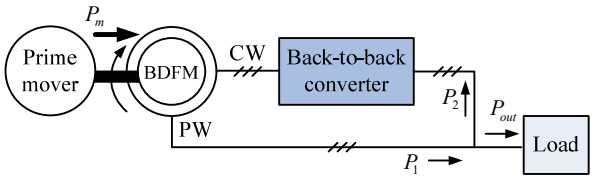

(a) Below the natural synchronous speed.

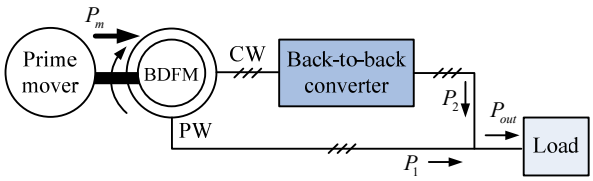

(b) Above the natural synchronous speed.

Fig. 5. Power flow of a stand-alone BDFIG operation system.

ignoring both the PW resistance R_1 and the CW resistance R_2'' yields:

$$\begin{aligned} P_1 &= 3\,\mathrm{Re}\left\{\frac{-|\dot{U}_1|^2(Z_2+Z_m)^* + (s_2/s_1)\dot{U}_1(\dot{U}_2''Z_m)^*}{[(Z_1+Z_2)Z_m+Z_1Z_2]^*}\right\} \\ &= 3\,\mathrm{Re}\left\{\frac{j|\dot{U}_1|^2(\alpha_2+L_{\sigma 2}''+\alpha_3)] - j\alpha_3(s_2/s_1)\dot{U}_1\dot{U}_2''^*}{-\omega_1(\alpha_1+L_{\sigma 1}+\alpha_2+L_{\sigma 2}'')\alpha_3 - \omega_1(\alpha_1+L_{\sigma 1})(\alpha_2+L_{\sigma 2}'')}\right\} \\ &= -3\alpha_3\frac{s_2}{s_1}\,\mathrm{Re}\left\{\frac{j\dot{U}_1\dot{U}_2''^*}{-\omega_1(\alpha_1+L_{\sigma 1}+\alpha_2+L_{\sigma 2}'')\alpha_3 - \omega_1(\alpha_1+L_{\sigma 1})(\alpha_2+L_{\sigma 2}'')}\right\} \end{aligned} \tag{18}$$

Substituting Eqns. (9)-(11) and (15) into Equ. (17), and ignoring R_1 and R_2'' leads to:

$$\begin{aligned} P_2 &= 3\,\mathrm{Re}\left\{\frac{-|\dot{U}_2|^2(s_2/s_1)(Z_1+Z_m)^* + \dot{U}_2''(\dot{U}_1Z_m)^*}{[(Z_1+Z_2)Z_m+Z_1Z_2]^*}\right\} \\ &= 3\,\mathrm{Re}\left\{\frac{j|\dot{U}_1|^2(s_2/s_1)(\alpha_1+L_{\sigma 1}+\alpha_3)] - j\alpha_3\dot{U}_1^*\dot{U}_2''}{-\omega_1(\alpha_1+L_{\sigma 1}+\alpha_2+L_{\sigma 2}'')\alpha_3 - \omega_1(\alpha_1+L_{\sigma 1})(\alpha_2+L_{\sigma 2}'')}\right\} \\ &= -3\alpha_3\,\mathrm{Re}\left\{\frac{j(\dot{U}_1\dot{U}_2''^*)^*}{-\omega_1(\alpha_1+L_{\sigma 1}+\alpha_2+L_{\sigma 2}'')\alpha_3 - \omega_1(\alpha_1+L_{\sigma 1})(\alpha_2+L_{\sigma 2}'')}\right\} \end{aligned} \tag{19}$$

From Eqns. (18) and (19), it can be obtained that:

$$\frac{P_1}{P_2} = -\frac{s_2}{s_1} \tag{20}$$

Considering Eqns. (5) and (20), it is derived that:

$$\frac{P_1}{P_2} = \frac{\omega_1}{\omega_2} \tag{21}$$

When a BDFIG is used in a stand-alone generation system, the PW always outputs power. However, below the natural synchronous speed ω_N, the CW will absorb power from the PW, because ω_2 is negative from Equ. (2), which means that the directions of the power flow in the PW and CW are opposite according to Equ. (21). Similarly, above ω_N, the CW will output power to the load.

The power flow of the system is shown in Fig. 5, where P_m is the mechanical input power from the prime mover, P_{out} is the active power output to the load, P_1 is the PW active power, and P_2 is the CW active power. If the active power injected to the windings is defined as a negative value, and the active power extracted from the windings is defined as a positive value, the power balance equation will be the same both below and above the natural synchronous speed, which can be expressed as:

$$P_m = P_1 + P_2 = P_{out} \tag{22}$$

According to Eqns. (2), (21), and (22), the capacity of the power converter for the stand-alone BDFIG system can be determined by considering the rotor speed range, the rated power factor, and P_{out}.

C. Steady-state Analysis of the CW Current

When the generator operates under the unloaded condition, $\dot{I}_1$ is nearly zero. From Equ. (12), the CW current under the unloaded condition, $\dot{I}_{2,\,\mathrm{unloaded}}''$, is expressed as:

$$\dot{I}_{2,\mathrm{unloaded}}'' = \frac{1}{Z_m}\dot{U}_1 = \frac{L_{m1}+L_{\sigma r}'+L_{m2}''}{j\omega_1 L_{m1}L_{m2}''}\dot{U}_1 \tag{23}$$

From Equ. (23), $\dot{I}_{2,\mathrm{unloaded}}''$ is independent of the rotor speed. The amplitude of the unreferred $\dot{I}_{2,\mathrm{unloaded}}$ is:

$$|\dot{I}_{2,\mathrm{unloaded}}| = \frac{n_1}{n_2}|\dot{I}_{2,\mathrm{unloaded}}''| = \frac{n_2(L_{m1}+L_{\sigma r}'+L_{m2}'')}{n_1\omega_1 L_{m1}L_{m2}''}|\dot{U}_1| \tag{24}$$

where n_1 is the ratio of the stator to the rotor turns for the PW, and n_2 is the ratio for the CW. Based on Equ. (24), if the amplitude of $\dot{U}_1$ is invariable, then $|\dot{I}_{2,\mathrm{unloaded}}|$ is constant at different rotor speeds.

Generally, from Equ. (12), the referred CW current $\dot{I}_2''$ under load can be expressed as:

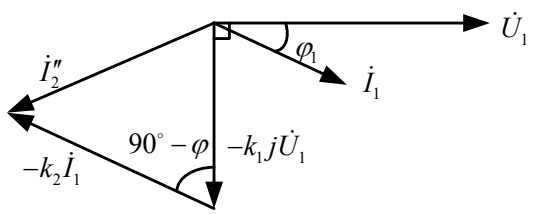

Fig. 6. Phasor diagram derived from Equ. (26).

$$\begin{aligned} \dot{I}_2'' &= \frac{1}{Z_m}\dot{U}_1 - \frac{Z_1+Z_m}{Z_m}\dot{I}_1 \\ &= \frac{L_{m1}+L_{\sigma r}'+L_{m2}''}{j\omega_1 L_{m1}L_{m2}''}\dot{U}_1 \\ &\quad - \frac{(R_1+j\omega_1 L_{\sigma 1})(L_{m1}+L_{\sigma r}'+L_{m2}'') + j\omega_1 L_{m1}(L_{\sigma r}'+L_{m2}'')}{j\omega_1 L_{m1}L_{m2}''}\dot{I}_1 \end{aligned} \tag{25}$$

If the PW resistance R_1 is ignored, the referred CW current $\dot{I}_2''$ can be further simplified as:

$$\dot{I}_2'' = -k_1 j\dot{U}_1 - k_2\dot{I}_1 \tag{26}$$

where $k_1 = \dfrac{L_{m1} + L'_{\sigma r} + L''_{m2}}{\omega_1 L_{m1} L''_{m2}}$,

$k_2 = \dfrac{L_{\sigma 1}(L_{m1} + L'_{\sigma r} + L''_{m2}) + L_{m1} L'_{\sigma r} + L_{m1} L''_{m2}}{L_{m1} L''_{m2}}$.

If the PW power factor is $\cos\varphi_1$, a phasor diagram derived from Equ. (26) can describe the relation between $\dot{U}_1$, $\dot{I}_1$, and $\dot{I}''_2$, as shown in Fig. 6. According to the Cosine Law, the amplitude of the CW current is:

$$|\dot{I}_2| = n_1 \sqrt{(k_1 |\dot{U}_1|)^2 + (k_2 |\dot{I}_1|)^2 - 2k_1 k_2 |\dot{U}_1||\dot{I}_1| \sin\varphi_1} \big/ n_2 \quad (27)$$

Considering that $n_r = 60\dfrac{\omega_r}{2\pi}$, $f_1 = \dfrac{\omega_1}{2\pi}$, and $f_2 = \dfrac{\omega_2}{2\pi}$, from Eqns. (2), (21), and (22), it can be obtained that:

$$P_1 = \frac{60 f_1}{n_r (p_1 + p_2)} P_{out} \quad (28)$$

where n_r is the rotor speed in r/min, while f_1 and f_2 are current frequencies of the PW and CW, respectively.

It should be noted that:

$$P_1 = 3 |\dot{U}_1||\dot{I}_1| \cos\varphi_1 \quad (29)$$

Combining Eqns. (28) and (29), the amplitude of the PW current $|\dot{I}_1|$ can be finally expressed as:

$$|\dot{I}_1| = \frac{20 f_1}{n_r (p_1 + p_2) |\dot{U}_1| \cos\varphi_1} P_{out} \quad (30)$$

If the load power factor is $\cos\varphi_L$ and the load impedance is Z_L, the BDFIG's output active power P_{out} can be expressed as:

$$P_{out} = 3 |\dot{U}_1|^2 \cos\varphi_L / |Z_L| \quad (31)$$

By substituting Equ. (31) into Equ. (30), the amplitude of the PW current $|\dot{I}_1|$ can be derived as follows:

$$|\dot{I}_1| = m |\dot{U}_1| \quad (32)$$

where $m = \dfrac{60 f_1 \cos\varphi_L}{n_r (p_1 + p_2) \cos\varphi_1 |Z_L|}$. m is constant when the generator's rotor speed and load are constant. According to Eqns. (27) and (32), the CW current under the loaded condition can be calculated by the following expression:

$$|\dot{I}_2| = n_1 |\dot{U}_1| \sqrt{k_1^2 + k_2^2 m^2 - 2k_1 k_2 m \sin\varphi_1} \big/ n_2 \quad (33)$$

By using Eqns. (24) and (33), it is possible to predetermine the steady-state amplitude of the CW current under the unloaded and loaded conditions.

V. Experimental Investigations

A. Experimental Setup

To investigate the performance of the stand-alone BDFIG operation system, an experimental setup has been established, as shown in Fig. 7. All of the experiments are performed on a prototype BDFIG, whose detailed parameters are listed in

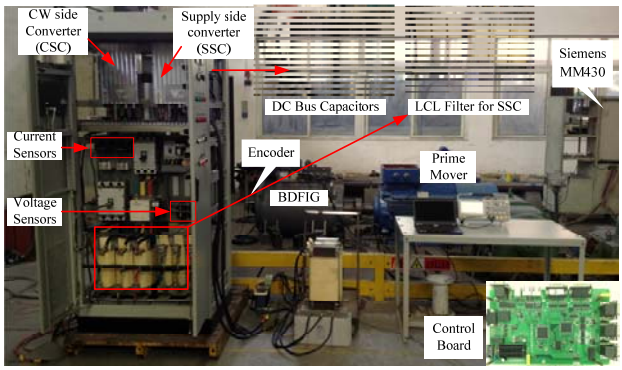

Fig. 7. Photograph of the experimental setup.

Table I. A 37 kW three-phase AC asynchronous motor as the prime mover is mechanically coupled to the BDFIG and driven by a Siemens MM430 converter. Four film capacitors are connected in parallel to the DC bus, and each capacitor has a capacitance of 4000uF and a rated DC voltage of 800V. The voltages and currents of the PW and CW are measured by LEM LV 100 and LEM LT 208-S7/SP1 sensors, respectively. The position of the rotor is measured by an incremental encoder (RHI90 from P+F Co.) with a resolution of 1024 cycles/r. The controller board is designed on basis of an ARM (Freescale MK60FN1M0VLQ12) and a FPGA (Altera Cyclone IV). A load cabinet provides the loads required for the generator with six sets of three-phase symmetrical resistances of 100 Ω each phase.

The control scheme is implemented by the double closed-loop control system based on the PW voltage and CW current. The cycle time of the program is 250 μs, and all of the control parameters are tuned through experiments. A detailed description of the control scheme has been presented

TABLE I.
PROTOTYPE BDFIG SPECIFICATION.

Parameter	Value	Parameter	Value
Frame size	D250	R_1	0.4036 Ω
PW pole pairs	1	R''_2	0.4430 Ω
CW pole pairs	3	R'_r	0.7852 Ω
Natural synchronous speed	750 r/min	$L_{\sigma 1}$	4.321 mH
Speed range	600~1500 r/min	$L''_{\sigma 2}$	2.199 mH
PW rated voltage	400 V	$L'_{\sigma r}$	8.217 mH
PW rated current	40 A	L_{m1}	470.8 mH
CW rated voltage	380 V	L''_{m2}	50.98 mH
CW rated current	40A	Rotor design	Wound rotor

in [22].

B. Improvement of the Start-Up Scheme for a Stand-Alone BDFIG System

Since the DC bus capacitors are uncharged before the

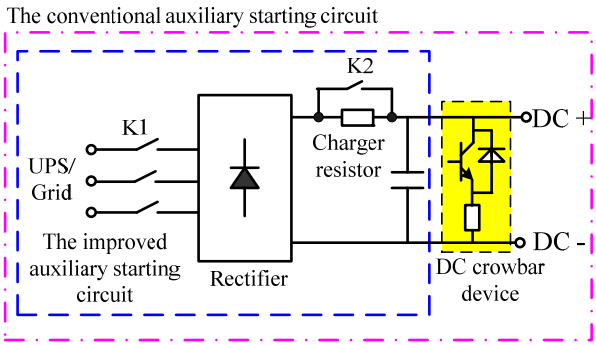

Fig. 8. Auxiliary circuit for starting a stand-alone BDFIG system.

stand-alone BDFIG system startup, the CSC cannot run or provide the CW with exciting current. Thus, an auxiliary circuit should be added to the system to pre-charge the DC bus capacitors. The conventional auxiliary circuit for the starting of the stand-alone BDFIG system is shown in Fig. 8. The start-up process of the stand-alone BDFIG operation system can be summarized as follows. First of all, the switch K1 is turned on and the rectifier begins to work. The charger resistor ensures that the charging current will not be too large. Then when the DC bus voltage is stabilized, the switch K2 is turned on to shorten the charger resistor. After that the CSC starts running to supply the CW with exciting current. Next, the SSC is started after the PW voltage rises to the set point. Finally, the switches K1 and K2 are turned off and the whole start-up process ends. Since the SSC is started after the CSC begins working, in the conventional auxiliary circuit, a DC crowbar device is used to avoid an excessively high DC bus voltage from the power output of the CW above the natural synchronous speed.

According to Eqns. (21) and (22), the CW active power can be expressed as:

$$P_2 = \omega_2 P_{out} / (\omega_1 + \omega_2) \tag{34}$$

Generally, in practical applications, a stand-alone BDFIG system is started without loads. Under the unloaded condition, P_{out} is zero. Thus, P_2 is zero at different rotor speeds, indicating that the power flow between the CW and the back-to-back converter is zero. Therefore, at no load, the BDFIG-based stand-alone power generation system can be started both below and above the natural synchronous speed without the power output of the CW. Therefore, the DC crowbar device can be removed to reduce the system cost. The improved auxiliary circuit for the stand-alone BDFIG system starting is also shown in Fig. 8.

In addition, the analysis results from Section IV show that when the generator runs under the unloaded condition, the CW current amplitude can be invariable to obtain a constant PW voltage amplitude and frequency at different rotor speeds. Therefore, according to Equ. (24), a constant CW current amplitude command can be used as a feedforward quantity in the controller at any rotor speeds when the stand-alone BDFIG system is started. Given this, the start-up speed of the stand-alone BDFIG system can be improved.

C. Experimental Results and Analysis

1) Experiment A

Fig. 9 shows the active power of the PW and CW of the prototype BDFIG under different load conditions, rotor speeds, and PW line voltages. The calculated values are obtained by using Eqns. (21) and (22). The experimental results are gained by the measured voltage and current of the PW and CW as well as the equations $P_1 = 3|\dot{U}_1||\dot{I}_1|\cos\varphi_1$ and $P_2 = 3|\dot{U}_2||\dot{I}_2|\cos\varphi_2$. As can be seen from Fig. 9, the experimental results are in good agreement with the calculated results. However, the sum of the experimental active power of the PW and CW is a little larger than P_{out} (the active power of the loads). The main reason for this is the active power loss in the two back-to-back converters. The natural synchronous speed of the prototype BDFIG, n_N, is 750 r/min. It can be found that active power flows into the CW below n_N and that it flows out of the CW above n_N. This means that the CW consumes power below n_N and outputs power to the loads above n_N.

2) Experiment B

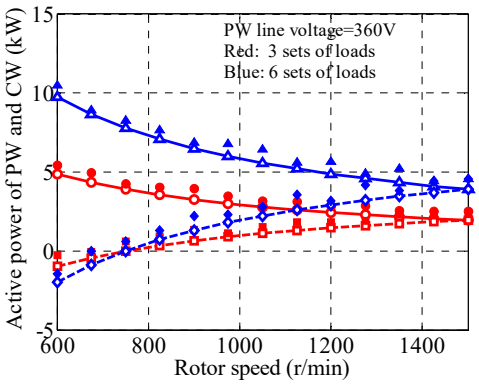

(a) PW line voltage of 360 V.

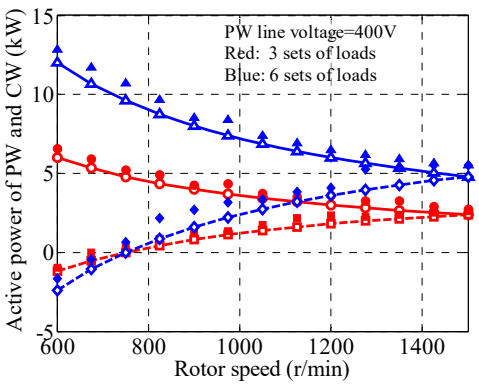

(b) PW line voltage of 400 V.

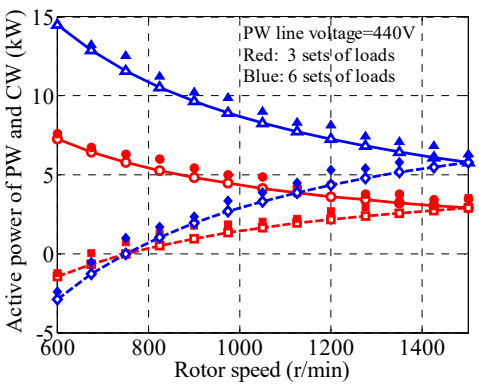

(c) PW line voltage of 440 V.

Fig. 9. Active power of the PW and CW under different loaded conditions, rotor speeds, and PW voltages. Each set of loads is a three-phase symmetrical resistance of 100 Ω for each phase.

Calculated:

○: PW active power under three sets of loads.

□: CW active power under three sets of loads.

Δ: PW active power under six sets of loads.

◇ : CW active power under six sets of loads.

Experimental:

●: PW active power under three sets of loads.

■: CW active power under three sets of loads.

▲: PW active power under six sets of loads.

◆: CW active power under six sets of loads.

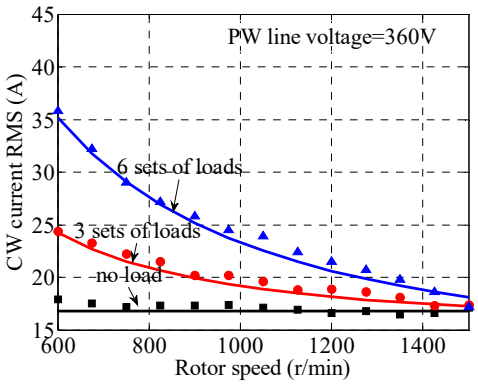

(a) PW line voltage of 360 V.

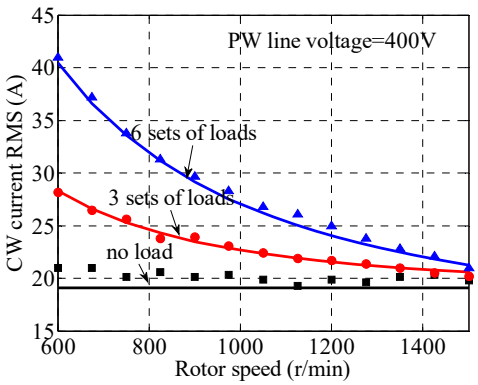

(b) PW line voltage of 400 V.

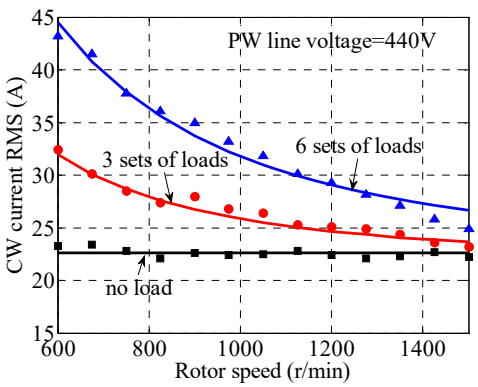

(c) PW line voltage of 440 V.

Fig. 10. CW rms current under different load conditions, rotor speeds, and PW line voltages. Each set of loads is a three-phase symmetrical resistance of 100 Ω for each phase.

Calculated:

black line: no load; red line: three sets of loads; blue line: six sets of loads.

Experimental:

■: no load; ●: three sets of loads; ▲: six sets of loads.

The CW rms current of the prototype BDFIG under different load conditions, rotor speeds, and PW line voltages are given in Fig. 10. The calculated results are obtained by using Eqns. (24) and (33). The experimental results match the calculated results very well, which verifies the validity of Eqns. (24) and (33). As shown in Fig. 10, at no load, the CW

rms current under different rotor speeds is almost the same, which meets the analysis results in Section IV. When loads are connected with the BDFIG, the CW rms current decreases with an increasing rotor speed during the entire speed range. This means that the load-carrying capacity of the generation system is stronger at higher speeds. In fact, when the generator is operating at a 600 r/min rotor speed under six sets of loads and a 400 V PW line voltage, the CW rms current is over 40 A (the CW rated current). However, it is just 22 A at a 1500 r/min rotor speed under the same load condition and PW line voltage.

Experiments A and B indicate that the stand-alone BDFIG operation system has better performance above natural synchronous speeds. Therefore, in stand-alone generation systems, the BDFIG should work above the natural synchronous speed as much as possible.

VI. Conclusion

This paper investigated the performance characteristics of stand-alone BDFIG operation systems. A new T-type steady-state model for BDFIGs is developed, which is more concise than the conventional Π-type steady-state model and more suitable for the analysis of stand-alone BDFIGs. Then based on the T-type steady-state model, the power flow of the stand-alone BDFIG operation system is investigated through detailed mathematical derivation. In addition, the steady-state characteristics of the CW current in the stand-alone BDFIG are analyzed by means of theoretical calculation. The analyzed results show that the CW current amplitude under the unloaded condition is constant at different rotor speeds. The predictive equation for the CW current amplitude under different loads and rotor speeds is also derived. Operation experiments of the stand-alone BDFIG system have been carried out on a prototype BDFIG to confirm the validity of the theoretical analysis.

The analyzed results can contribute to improving the control systems for actual industrial applications. Firstly, the analyzed results of the power flow are useful to accurately determine the capacity of a power converter according to the rotor speed range and to simplify the auxiliary circuit for the starting of the stand-alone BDFIG. Secondly, the analyzed results of the CW current are helpful to accelerate BDFIG startup by adding an accurate CW current feedforward to the controller. Finally, all of the analyzed results show that, for the actual application of stand-alone power generation, a BDFIG should be selected whose natural synchronous speed is below the prime mover speed as much as possible.

Work is underway to further improve the dynamic performance of the stand-alone BDFIG system.

Appendix

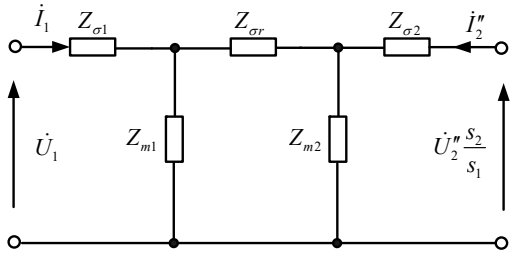

Fig. 11. Concise representation of the Π-type steady state model.

Derivation of the Parameters of the T-type Steady-State Model

In order to facilitate the derivation of the T-type steady-state model, the Π-type steady-state model shown in Fig. 1 is presented in a concise form, as shown in Fig. 11, where the model parameters are defined as:

$$\begin{cases} Z_{\sigma 1} = R_1 + j\omega_1 L_{\sigma 1} \\ Z_{\sigma r} = R_r' \big/ s_1 + j\omega_1 L_{\sigma r}' \\ Z_{\sigma 2} = R_2'' s_2 \big/ s_1 + j\omega_1 L_{\sigma 2}'' \\ Z_{m1} = j\omega_1 L_{m1} \\ Z_{m2} = j\omega_1 L_{m2}'' \end{cases} \tag{35}$$

The Π-type steady-state model shown in Fig. 11 is actually a passive linear two-port network, whose external characteristics can be described as follows [24]:

$$\begin{cases} \dot{U}_1 = Z_{11}\dot{I}_1 + Z_{12}\dot{I}_2'' \\ s_2\dot{U}_2'' / s_1 = Z_{21}\dot{I}_1 + Z_{22}\dot{I}_2'' \end{cases} \tag{36}$$

where Z_{11}, Z_{12}, Z_{21}, and Z_{22} are the open-circuit impedance parameters for the two-port network, and can be derived as follows [24]:

$$Z_{11} = \frac{\dot{U}_1}{\dot{I}_1}\Big|_{\dot{I}_2''=0} = \frac{Z_{m1}(Z_{\sigma r} + Z_{m2})}{Z_{m1} + Z_{\sigma r} + Z_{m2}} + Z_{\sigma 1} \tag{37}$$

$$Z_{21} = \frac{s_2\dot{U}_2'' / s_1}{\dot{I}_1}\Big|_{\dot{I}_2''=0} = \frac{Z_{m1}Z_{m2}}{Z_{m1} + Z_{\sigma r} + Z_{m2}} \tag{38}$$

$$Z_{12} = \frac{\dot{U}_1}{\dot{I}_2''}\Big|_{\dot{I}_1=0} = \frac{Z_{m1}Z_{m2}}{Z_{m1} + Z_{\sigma r} + Z_{m2}} \tag{39}$$

$$Z_{22} = \frac{s_2\dot{U}_2'' / s_1}{\dot{I}_2''}\Big|_{\dot{I}_1=0} = \frac{Z_{m2}(Z_{\sigma r} + Z_{m1})}{Z_{m1} + Z_{\sigma r} + Z_{m2}} + Z_{\sigma 2} \tag{40}$$

From Eqns. (38) and (39), it can be seen that $Z_{12} = Z_{21}$. Then rearranging Equ. (36), the external characteristics of the Π-type steady-state model can be rewritten as:

$$\begin{cases} \dot{U}_1 = (Z_{11} - Z_{12})\dot{I}_1 + Z_{12}(\dot{I}_1 + \dot{I}_2'') \\ s_2\dot{U}_2'' / s_1 = Z_{12}(\dot{I}_1 + \dot{I}_2'') + (Z_{22} - Z_{12})\dot{I}_2'' \end{cases} \tag{41}$$

According to Ohm's law, the following expression can be obtained from the T-type steady-state model as shown in Fig. 3:

$$\begin{cases} \dot{U}_1 = Z_1\dot{I}_1 + Z_m(\dot{I}_1 + \dot{I}_2'') \\ s_2\dot{U}_2'' / s_1 = Z_m(\dot{I}_1 + \dot{I}_2'') + Z_2\dot{I}_2'' \end{cases} \tag{42}$$

Comparing Eqns. (41) and (42), the following results are obtained:

$$\begin{cases} Z_1 = Z_{11} - Z_{12} \\ Z_2 = Z_{22} - Z_{12} \\ Z_m = Z_{12} \end{cases} \tag{43}$$

By substituting Eqns. (37)-(40) into Equ. (43), the relations between the T-type and Π-type steady-state model can be derived as:

$$\begin{cases} Z_1 = \dfrac{Z_{m1}Z_{\sigma r}}{Z_{m1} + Z_{\sigma r} + Z_{m2}} + Z_{\sigma 1} \\ Z_2 = \dfrac{Z_{m2}Z_{\sigma r}}{Z_{m1} + Z_{\sigma r} + Z_{m2}} + Z_{\sigma 2} \\ Z_m = \dfrac{Z_{m1}Z_{m2}}{Z_{m1} + Z_{\sigma r} + Z_{m2}} \end{cases} \tag{44}$$

Then the Eqns. (6)-(8) for the parameters of the T-type steady-state model can be obtained by substituting Equ. (35) into Equ. (44).

REFERENCES

[1] S. Shao, E. Abdi, F. Barati, and R. A. McMahon, "Stator-flux-oriented vector control for brushless doubly-fed induction generator," *IEEE Trans. Ind. Electron.*, Vol. 56, No. 10, pp. 4220-4228, Oct. 2009.

[2] T. Logan, J. Warrington, S. Shao, and R. McMahon, "Practical deployment of the Brushless Doubly-Fed Machine in a medium scale wind turbine", in *Proc. Int. Conf. Power Electronics and Drive Systems (PEDS)*, pp. 470-475, 2009.

[3] S. Shao, A. Ehsan, and R. McMahon, "Vector control of the brushless doubly-fed machine for wind power generation," in *Proc. Int. Conf.* Sustainable Energy Technol., pp. 322-327, 2008.

[4] S. Ademi and M. G. Jovanovic, "High-efficiency control of brushless doubly-fed machines for wind turbines and pump drives," *Energy Convers. Manage.*, Vol. 85, No. 5, pp. 120-132, May 2014.

[5] K. Vijayakumar, N. Kumaresan, and N. Ammasai Gounden, "Operation and closed-loop control of wind-driven stand-alone doubly fed induction generators using a single inverter-battery system," *IET Electr. Power Appl.*, Vol. 6, No. 3, pp. 162-171, 2012.

[6] K. Vijayakumar, N. Kumaresan, and N. Ammasai Gounden, "Operation of inverter-assisted wind-driven slip-ring induction generator for stand-alone power supplies," *IET Electr. Power Appl.*, Vol. 7, No. 4, pp. 256-269, 2013.

[7] Van-Tung Phan and Hong-Hee Lee, "Enhanced Proportional-Resonant Current Controller for Unbalanced Stand-alone DFIG-based Wind Turbines," *Journal of Electrical Engineering & Technology*, Vol. 5, No. 3, pp. 443-450, 2010.

[8] Yung-Deug Son, Won-Sang Im, Han-Seok Park and Jang-Mok Kim, "Analysis and Compensation of Current Measurement Errors in a Doubly Fed Induction Generator," *Journal of Electrical Engineering & Technology*, Vol. 9, No. 2, pp. 532-540, 2014.

[9] D. Zhou, R. Spee, and A. K. Wallace, "Laboratory control implementations for doubly-fed machines," in *Proc. IEEE IECON*, Vol. 1, pp. 1181-1186, 1993.

[10] I. Sarasola, E. Oyarbide, D. Roye, and M. Rodriguez, "Stability analysis of a brushless doubly-fed machine under closed loop scalar current control," in *Proc. IEEE Ind. Electron. Society Conf.*, pp. 1527-1532, 2006.

[11] S. Shao, E. Abdi, and R. McMahon, "Low-cost variable speed drive based on a brushless doubly-fedmotor and a fractional unidirectional converter," *IEEE Trans. Ind. Electron.*, Vol. 59, No. 1, pp. 317-325, Jan. 2012.

[12] R. Li, R. Spee, A. K. Wallace, and G. C. Alexander, "Synchronous drive performance of brushless doubly-fed motors," *IEEE Trans. Ind. Appl.*, Vol. 30, No. 4, pp. 963-970, Jul./Aug. 1994.

[13] A. Zhang, X. Wang, W. Jia, and Y. Ma, "Indirect stator-quantities control for the brushless doubly fed induction machine," *IEEE Trans. Power Electron.*, Vol. 29, No. 3, pp. 1392-1401, Mar. 2014.

[14] I. Sarasola, J. Poza, M. A. Rodriguez, and G. Abad, "Direct torque control design and experimental evaluation for the brushless doubly fed machine," *Energy Convers. Manage.*, Vol. 52, No. 2, pp. 1226-1234, 2011.

[15] P. C. Roberts, R. A. McMahon, P. J. Tavner, J. M. Maciejowski, T. J. Flack, and X.Wang, "Performance of rotors for the brushless doubly fed (induction) machine (BDFM)," in *Proc. Int. Conf. Electr. Machines*, pp. 450-455, 2004.

[16] R. E. Betz and M. G. Jovanovic, "Theoretical analysis of control properties for the brushless doubly fed reluctance machine," *IEEE Trans. Energy Convers.*, Vol. 17, No. 3, pp. 332-339, Sept. 2002.

[17] F. Xiong and X. Wang, "Design of a low-harmonic-content wound rotor for the brushless doubly fed generator," *IEEE Trans. Energy Convers.*, Vol. 29, No. 1, pp. 158-168, Mar. 2014.

[18] R. A. McMahon, P. C. Roberts, X. Wang, and P. J. Tavner, "Performance of BDFM as generator and motor," *IEE Proc. Electr. Power. Appl.*, Vol. 153, No. 2, pp. 289-299, Mar. 2006.

[19] F. Xiong and X. Wang, "Design and performance analysis of a brushless doubly-fed machine for stand-alone ship shaft generator systems," in *Proc. IEEE Electr. Control Eng. Conf.*, pp. 2114-211, Sep. 2011.

[20] F. Xiong, "Research on modeling analysis and electromagnetic design of wound-rotor brushless doubly-fed machine," Ph.D. dissertation, Dept. Electr. Eng., Huazhong Univ. Sci. Tech., Wuhan, China, 2010.

[21] P. C. Roberts, R. A. McMahon, P. J. Tavner, J. M. Maciejowski, T. J. Flack, "Equivalent circuit for the brushless doubly fed machine (BDFM) including parameter estimation and experimental verification," *IEE Proc. Electr. Power. Appl.*, Vol. 152, No. 4, pp. 933-942, Jul. 2005.

[22] Y. Liu, W. Ai, B. Chen, and K. Chen, "Control design of the brushless doubly-fed machines for stand-alone VSCF ship shaft generator systems," *Journal of Power Electronics*, Vol. 16, No. 1, pp. 259-267, Jan. 2016.

[23] Y. Liu, W. Ai, B. Chen, K. Chen, "Control design and experimental verification of the brushless doubly-fed machine for stand-alone power generation applications," *IET Electric Power Applications*, Vol. 10, No. 1, pp. 25-35, 2016.

[24] A. B. Carlson, *Circuits: Engineering Concepts and Analysis of Linear Electric Circu*its, John Wiley & Sons, 1996.

ACKNOWLEDGMENT

The authors would like to thank China Changjiang National Shipping Group Motor Factory for providing the prototype BDFIG.

Yi Liu was born in Wuhan, China, in 1982. He received his B.S. and M.S. degrees in Automation and Control Engineering from the Wuhan University of Science and Technology, Wuhan, China, in 2004 and 2007, respectively; and his Ph.D. degree in Mechatronic Engineering from the Huazhong University of Science and Technology, Wuhan, China, in 2016. From 2007 to 2011, he was a Lecturer at the Wuhan University of Science and Technology. From March 2016 to June 2016, he was a Senior R & D Engineer at the Fourth Academy of China Aerospace Science and Industry Group, Wuhan, China. In July 2016, he became a Lecturer in the School of Mechanical and Electrical Engineering, Huanggang Normal University, Huanggang, China. His current research interests include AC electrical machine control and inverter systems.

Wei Xu was born in Chongqing, China, in 1980. He received his B.S. and M.S. degrees from Tianjin University, Tianjin, China, in 2002 and 2005, respectively; and his Ph.D. degree from the Institute of Electrical Engineering, Chinese Academy of Sciences, Beijing, China, in 2008, all in Electrical Engineering. From 2008 to 2012, he held several positions in Australian and Japanese universities and companies. Since 2013, he has been full Professor in the School of Electrical and Electronic Engineering, Huazhong University of Science and Technology, Wuhan, China. His current research interests include electromagnetic designs and control algorithms for linear/rotary machines, including induction, permanent magnet, double salient, and other emerging novel structure machines.

Gang Zhi was born in Shaanxi Province, China, in 1982. He received his B.S. degree from the Hubei University of Technology, Wuhan, China, in 2009; and his M.S. degree from the Huazhong University of Science and Technology, Wuhan, China, in 2015, all in Electrical Engineering. From 2005 to 2016, he was an R&D Engineer with the China Changjiang National Shipping Group Motor Factory, Wuhan, China. In January 2017, he bacame the Director of the R&D department of Wuhan Yanghua Electric Co., Ltd, Wuhan, China. His current research interests include brushless doubly-fed machine designs and drives.

Junlin Zhang was born in Hubei Province, China, in 1982. He received his B.S. degree in Mechanical Engineering from Yangtze University, Jingzhou, China, in 2006. He is presently working towards his M.S. degree in the School of Mechanical Engineering, Hubei University of Technology, Wuhan, China. In July 2006, he bacame an Assistant in the School of Mechanical and Electrical Engineering, Huanggang Normal University, Huanggang, China. His current research interests include electrical drives and machine control.